fluids

MDPI

Article

A Calculation Method and Application Research in Gas-Lift Reverse Circulation Bottom-Hole Pressure Based on Gas–Liquid Two-Phase Flow Theory

Pu Liu [1,*], Chuanhua Ge [1], Ruiqi Zhang [1], Ruifeng Tan [2] and Shanquan Fan [3]

[1] School of Mechanical Engineering, Yibin Campus, Sichuan University of Science and Engineering, Yibin 644005, China
[2] Sinopec Huadong Oilfield Service Corporation, Nanjing 210019, China
[3] China National Petroleum Corporation Jidong Oilfield Company, Tangshan 063004, China
* Correspondence: g32015629841@163.com

Abstract

Gas-lift reverse circulation drilling technology is one of the typical "bottom-hole negative pressure" drilling technologies. This technology can significantly reduce wellbore circulation pressure loss, alleviate the bottom-hole pressure holding effect, and effectively lower the probability of lost circulation. The core theory underlying this technology is multiphase flow in the wellbore. Based on gas–liquid two-phase flow theory, this paper develops a method for calculating bottom-hole pressure during gas-lift reverse circulation. The effects of key operational parameters on bottom-hole pressure were analyzed. The results show that bottom-hole pressure decreases as gas injection rate increases and as the gas injection point deepens. Moreover, the deeper the gas injection point, the greater the pressure reduction. Compared with the results from gas-lift reverse circulation drilling design and monitoring software applied to a shale gas well in southern Sichuan, the two sets of data differ by approximately 3%. The proposed calculation method can predict bottom-hole pressure under gas-lift reverse circulation conditions, overcoming the low accuracy of empirical formulas traditionally used in such operations. This has significant implications for advancing gas-lift reverse circulation technology in oil and gas well drilling.

Keywords: gas-lift reverse circulation; gas–liquid two-phase flow; bottom-hole pressure; wellbore leakage

Academic Editors: Akira Nakayama, Miao Chen, Xiangxiang Zhang and Shiliang Liu

Received: 30 March 2026
Revised: 28 April 2026
Accepted: 11 May 2026
Published: 14 May 2026

1. Introduction

In the field of oil and gas drilling, particularly for shale gas development in karst terrains, shallow fractures and caves are well-developed, while the deep layers have undergone multiple stages of tectonic superimposed deformation [1]. The geological conditions are complex, with abnormal development of fractures and sinkholes, and a complicated fault system. During the 'bottom-hole positive pressure' [2] drilling process, wellbore leakage is highly likely. In 2022, a total of 60 instances of wellbore leakage occurred across 19 wells in the western Chongqing shale gas block, with severe loss primarily caused by three-stage losses [3]. Among them, total loss of returns occurred in 24 instances (14 of which were in the Jialingjiang Formation), while medium and small losses occurred in 36 instances. The leakage range was extensive, and the overall leakage situation was complex. A total of 20,920.86 h of drilling time were lost, and the total volume of lost drilling fluid was 47,126.72 m^3. The average loss time per well was 1101 h, and the average

loss volume per well was 2480 m^3. The loss of returns was the primary issue, with the Jialingjiang Formation experiencing the most severe leakage. After successful pressure cementing and leak plugging in the Jialingjiang Formation, the recurrence of leakage typically occurred every 30 days. During drilling through the lower high-pressure layers, after the recurrence of leakage in the upper wellbore section, the leakage rate was relatively high. The loss of returns accounted for 60% of the total leakage.

Therefore, to avoid or reduce wellbore leakage and other issues [4], the 'bottom-hole positive pressure' is often replaced with 'bottom-hole negative pressure' [5]. Gas-lift reverse circulation technology is one of the processes that use 'bottom-hole negative pressure.' This technology significantly reduces the circulation pressure consumption at the bottom of the well, effectively protecting the wellbore stability and reducing the risk of wellbore leakage [6,7]. Currently, gas-lift circulation drilling technology is still in its early stages in the field of oil and gas well drilling [8]. The calculation of key parameters for gas-lift reverse circulation technology still relies on the experience summarized by previous researchers, and has not yet formed a systematic theoretical framework. This has led to inaccurate control of bottom-hole pressure [9].

The core theory of the gas-lift reverse circulation process lies in the multiphase flow theory within the wellbore [10]. Currently, gas–liquid two-phase flow is widely present in many fields (such as chemical engineering, petroleum, medical, and biological fields) [11,12], and therefore, researchers have conducted in-depth studies on the flow characteristics of gas in liquids.

Chengcheng Luo developed an accurate model for predicting the pressure gradient of gas–liquid two-phase flow based on the Mukherjee–Brill model. Voke Salubi [13] studied the effect of drilling parameters on the flow patterns of gas–liquid two-phase flow and proposed a method for evaluating cuttings transport efficiency and performing underbalanced drilling hydraulics calculations based on the flow patterns. Wenbo Zhang [14] developed a wellbore multiphase flow model that considers gas dissolution and suspension, and analyzed the impact of gas dissolution and suspension on drilling fluid overflow, wellbore shutdown, and compression processes. Jingmeng Tian [15] conducted experimental and theoretical calculations to study the effect of gas content and flow rate on the pressure within the wellbore. Jie Zheng [16] based on the wellbore gas–liquid two-phase flow theory and heat transfer theory, developed a temperature–pressure coupling prediction model for high-water-content gas wells, which helps better predict the temperature–pressure coupling conditions in the wellbore of high-water-content gas wells. Wei [17] developed a multiphase flow mathematical model based on underbalanced drilling conditions and studied the properties of crude oil in high-temperature, high-pressure formations. In summary, many scholars both domestically and internationally have established various gas–liquid two-phase flow models in the field of oil and gas wells [18]. However, these models are only applicable to general conditions such as underbalanced drilling and pressure control drilling [19]. Systematic research on wellbore gas–liquid two-phase flow under the special condition of gas-lift reverse circulation has not been conducted.

This paper mainly proposes a calculation method for predicting the injection point pressure and bottom-hole pressure under gas-lift reverse circulation, based on the gas–liquid two-phase flow theory. The method involves fine regional division of the wellbore and iterative solving of parameters within the wellbore. A calculation model for predicting bottom-hole pressure is established, which can estimate the impact of different injection point locations, gas injection volumes, and other parameters on bottom-hole pressure. The research results have certain reference value for improving the accuracy of bottom-hole pressure control in gas-lift reverse circulation drilling.

2. Bottom-Hole Pressure Calculation Model

In gas-lift reverse circulation drilling, the wellbore fluid can be divided into three parts: the bottom-hole zone (liquid-solid two-phase), the gas-lift zone (gas–liquid-solid three-phase), and the wellhead zone, as shown in Figure 1.

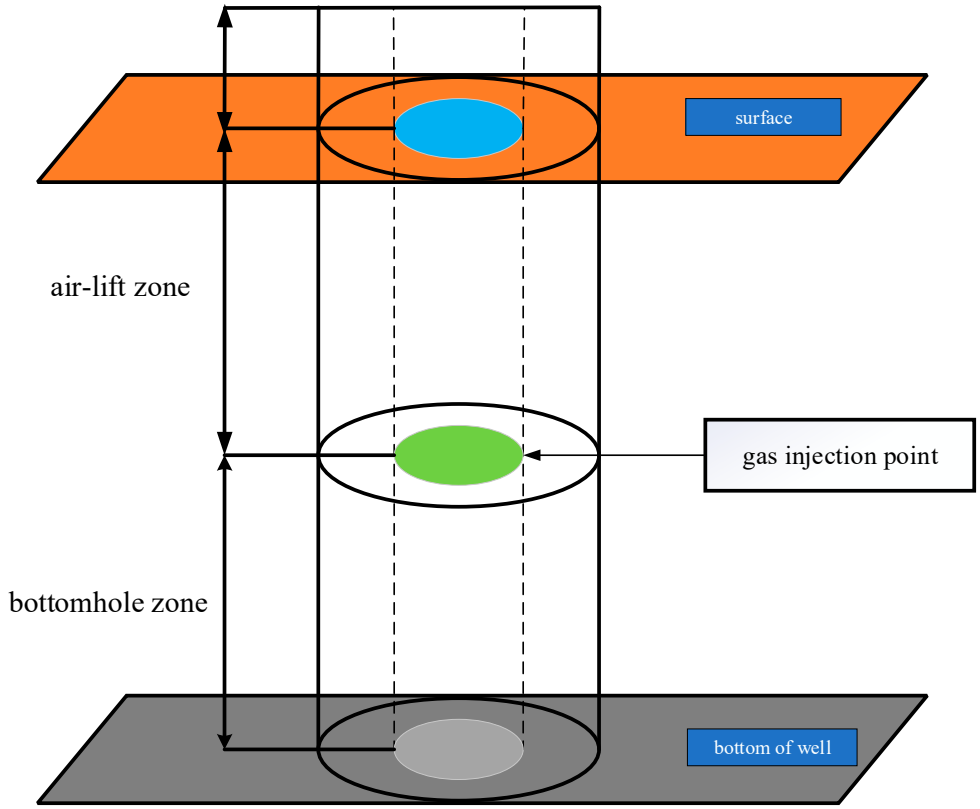

Figure 1. Gas-Lift Reverse Circulation Zones.

Due to the complex fluid flow within the wellbore during actual drilling, the following assumptions are made:

(1) The effect of drill string rotation on the drilling fluid flow is not considered.
(2) The temperature follows the geothermal gradient, and heat transfer is ignored.
(3) Drilling fluid is considered to be an incompressible liquid.
(4) The distribution of cuttings in the drilling fluid is assumed to be uniform, and the effect of cuttings on pressure is not considered. The pressure is calculated based on gas–liquid two-phase flow in the gas-lift zone and single-phase flow of drilling fluid in the bottom-hole zone.

Although these assumptions neglect drill string rotation and complex heat transfer, their impact on bottom-hole pressure calculation is limited under the shallow-to-intermediate gas-lift reverse circulation conditions evaluated in this study. Regarding rotation, the two-phase flow of interest occurs inside the drill pipe, where the axial pressure drop is dominated by bulk velocity; the tangential swirl induced by pipe rotation contributes less than 2% to inner-wall friction loss. Regarding heat transfer, given the shallow injection depths considered (<1600 m), the temperature variation along the wellbore is modest, and gas expansion cooling partially offsets geothermal heating, making the linear geothermal profile a reasonable first-order approximation. The 3% error benchmarked against field software in Section 4.3 substantiates the controllability of these simplifications.

Gas dissolution into the drilling fluid is neglected in the current model. Under elevated pressures, a fraction of the injected gas may dissolve into the liquid phase, reducing the free

gas holdup and thereby the pressure reduction capacity. For the conditions in this study, the solubility of air in water is approximately 0.02–0.04 kg/m^3 per MPa, resulting in a maximum dissolved gas volume fraction of less than 2% of the injected gas. A preliminary estimate suggests that neglecting dissolution may lead to an overestimation of bottom-hole pressure reduction by less than 5%. This error is within the overall accuracy of the model.

When the wellbore flow in gas-lift reverse circulation drilling reaches a steady state, the bottom-hole pressure is equal to the sum of the wellhead pressure, the pressure of the liquid column in the drill string, and the flow pressure loss.

$$P_{jd} = P_0 + P_{yh} + P_{yz} \tag{1}$$

In the gas-lift reverse circulation condition, the calculation of the liquid column pressure within the drill string consists of two parts: the single-phase section of drilling fluid in the bottom-hole zone and the gas–liquid two-phase mixed phase section in the gas-lift zone.

$$P_{yz} = P_{qy} + P_d \tag{2}$$

2.1. Gas-Lift Zone Gas–Liquid Two-Phase Flow Pressure Calculation Model

During the gas-lift reverse circulation drilling process, the fluid flow within the drill string above the gas-water mixer is a gas–liquid two-phase flow. Since the focus of this paper is on gas–liquid two-phase flow in vertical cylindrical pipes, the Hasan and Kabir model is chosen for the gas–liquid two-phase flow calculation.

Although the Hasan–Kabir model was originally developed for conventional upward two-phase flow in vertical tubing, its application to gas-lift reverse circulation is justified because: (1) the gas–liquid two-phase flow inside the drill string is also vertical upward flow, with the gas injected at the bottom of the gas-lift zone; (2) the flow direction and phase interaction mechanisms (bubble coalescence, slug formation, etc.) are physically similar; and (3) the model has been successfully validated against field data from reverse circulation operations, as shown in Section 4.3 with an error below 5%. No modification of the model coefficients is required for this configuration.

2.1.1. Liquid Column Pressure in Gas–Liquid Two-Phase Flow

For calculating the liquid column pressure in gas–liquid two-phase flow [20–22], the density at the calculation point should be the mixed density of the gas–liquid two-phase flow.

$$P_{qy} = \rho_m g \Delta h \tag{3}$$

The mixed density of the gas–liquid two-phase flow is

$$\rho_m = E_g \rho_g + (1 - E_g)\rho_l \tag{4}$$

2.1.2. Flow Pressure Loss in Gas–Liquid Two-Phase Flow

The apparent velocity of the gas phase is

$$V_{sg} = Q_g / A \tag{5}$$

The apparent velocity of the liquid phase is

$$V_{sl} = Q_l / A \tag{6}$$

The mixed velocity is

$$V_m = V_{sg} + V_{sl} \tag{7}$$

(1) Bubbly Flow

Bubbly Flow Identification:

$$v_{sg} < 0.429v_{sl} + 0.357v_{0\infty} \tag{8}$$

The density of a gas at any temperature T and pressure P can be determined from the ideal gas law:

$$\rho_g = \frac{pM_g}{ZRT} \tag{9}$$

Flow Pressure Loss of Bubble Flow:

$$\left(\frac{dp}{dz}\right)_{fr} = \frac{2f_m v_m^2 \rho_m}{D} \tag{10}$$

(2) Slug Flow

Slug Flow Identification:

$$\begin{gathered} v_{sg} > 0.429v_{sl} + 0.357v_{0\infty} \\ \rho_g v_{sg}^2 < 25.41g\left(\rho_l v_{sl}^2\right) - 38.9\left(\rho_l v_{sl}^2 > 74.4\right) \\ \rho_g v_{sg}^2 < 0.0051\left(\rho_l v_{sl}^2\right)^{1.7}\left(\rho_l v_{sl}^2 < 74.4\right) \end{gathered} \tag{11}$$

Flow Pressure Loss of Slug Flow:

$$\left(\frac{dp}{dz}\right)_{fr} = \frac{2v_m^2 \rho_m f_m}{D}\left(1 - E_g\right) \tag{12}$$

(3) Dispersed Flow

Dispersed Flow Identification:

$$\begin{gathered} v_{sg} < 3.1\left(\sigma g\left(\rho_l - \rho_g\right)/\rho_g^2\right)^{0.25} \\ \rho_g v_{sg}^2 > 25.41g\left(\rho_l v_{sl}^2\right) - 38.9\left(\rho_l v_{sl}^2 > 74.4\right) \\ \rho_g v_{sg}^2 > 0.0051\left(\rho_l v_{sl}^2\right)^{1.7}\left(\rho_l v_{sl}^2 < 74.4\right) \end{gathered} \tag{13}$$

In practice, the flow behavior between dispersed flow and slug flow is often very similar, and the distinction between the two in terms of their flow regimes is somewhat ambiguous. Therefore, in actual engineering applications, the dispersed flow and slug flow regimes are usually treated as the same, and handled according to the same standard.

(4) Annular Flow

Annular Flow Identification:

$$v_{sg} > 3.1\left[\frac{\sigma g\left(\rho_l - \rho_g\right)}{\rho_g^2}\right]^{0.25} \tag{14}$$

Flow Pressure Loss of Annular Flow:

$$\left(\frac{dp}{dz}\right)_{fr} = \frac{2v_g^2 \rho_c f_c}{D} \tag{15}$$

In the current implementation, the flow pattern is determined by the criteria listed above, and the corresponding pressure loss formula is applied directly. A hard switch at the transition boundary can theoretically cause a discontinuity in the pressure gradient. How-

ever, because the grid step size is small and the transition criteria are based on continuous variables (e.g., mixture velocity, gas holdup), the observed jump in pressure gradient is less than 2% across the transition depth. This is deemed acceptable for engineering predictions.

2.1.3. Gas Compressibility Factor Calculation

Due to the significant variation in the gas compressibility factor Z with pressure and temperature along the wellbore, an accurate determination of Z is essential for gas density calculation. In this study, the Z factor is computed iteratively using the Dranchuk–Abou-Kassem (DAK) correlation, which is expressed in terms of pseudo-reduced properties:

$$P_{pr} = \frac{P}{P_{pc}} \tag{16}$$

$$T_{pr} = \frac{T}{T_{pc}} \tag{17}$$

The Z factor is then obtained by solving the nonlinear DAK equation using the Newton–Raphson method within each grid cell of the wellbore discretization loop. The 11-constant form of the DAK correlation is employed, ensuring convergence and accuracy across the range of pressures and temperatures encountered in this work.

$$\begin{aligned} Z = \; & 1 + \left(A_1 + \frac{A_2}{T_{pr}} + \frac{A_3}{T_{pr}^3} + \frac{A_4}{T_{pr}^4} + \frac{A_5}{T_{pr}^5}\right)\rho_{pr} + \left(A_6 + \frac{A_7}{T_{pr}} + \frac{A_8}{T_{pr}^2}\right)\rho_{pr}^2 - A_9\left(\frac{A_7}{T_{pr}} + \frac{A_8}{T_{pr}^2}\right)\rho_{pr}^5 + \\ & A_{10}\left(1 + A_{11}\rho_{pr}^2\right)\left(\frac{\rho_{pr}^2}{T_{pr}^3}\right)\exp\left(-A_{11}\rho_{pr}^2\right) \end{aligned} \tag{18}$$

The injected gas in this study is assumed to be air, with a molar mass of 28.97 g/mol and a standard density of 1.21 kg/m^3 at 20 °C and 0.1 MPa. The critical properties used in the DAK correlation are P_c = 3.786 MPa and T_c = 132.5 K for air. The DAK correlation is valid for reduced pressures $0.2 \leq P_r \leq 15$ and reduced temperatures $1.0 \leq T_r \leq 3.0$, covering the full range of operating conditions in this study (maximum bottom-hole pressure is 25 MPa, maximum temperature is 95 °C).

2.2. Calculation of Pure Liquid Phase Pressure in the Wellbore Region

In the gas-lift reverse circulation condition, the flow below the gas–water mixer is a two-phase flow of liquid and solid. This paper neglects the effect of rock cuttings on pressure, and the pressure at the bottom of the well is calculated based on the pure liquid phase.

For the single-phase segment of the drilling fluid, the fluid density at the calculation point should be taken as the density of the drilling fluid.

$$P_d = \rho_l g h_2 \tag{19}$$

For the single-phase flow segment of the drilling fluid, the conventional Darcy's law can be used to calculate the pressure loss due to the flow of drilling fluid inside the drill pipe.

$$P_{fd} = \frac{2v_l^2 \rho_l f_l h_2}{D} \tag{20}$$

In the gas-lift reverse circulation drilling process, the fluid flow regime is regarded as laminar flow, and the Fanning friction factor is solved using the Bingham plastic model.

$$\begin{aligned} f_l &= \tfrac{24}{\mathrm{Re}_l} \\ \mathrm{Re}_l &= \frac{v_l D}{\mu_l + \frac{\tau_l D}{8 v_l}} \end{aligned} \tag{21}$$

Local pressure losses at the gas–water mixer, bottom-hole entry, and other tool joints are neglected in this model. These losses are typically one to two orders of magnitude smaller than the distributed friction loss along the drill string for the flow rates considered.

3. Calculation Method

The current model assumes a uniform inner diameter of the drill string. For practical drilling assemblies where the inner diameter varies along the bottom-hole assembly (BHA) or across special tools, the model can be extended by segmenting the wellbore into sections with different diameters. The finite difference method described below can accommodate such segmentation by assigning the appropriate diameter to each grid cell. For the case study presented, the drill string is assumed to have a constant inner diameter of 0.08 m, which is representative of a uniform pipe section.

The pure drilling fluid section is a single-phase flow, and the pressure calculation is simple. However, in the gas–liquid two-phase flow section, the pressure drop gradient changes with the flow pattern, making the pressure drop calculation more complex. Therefore, to ensure accurate calculation results, the finite difference method will be used to discretize the gas–liquid two-phase mixture in the gas-lift zone, as shown in Figure 2. Starting from the wellhead, several small sections with length ΔL are sequentially taken until the injection point is reached.

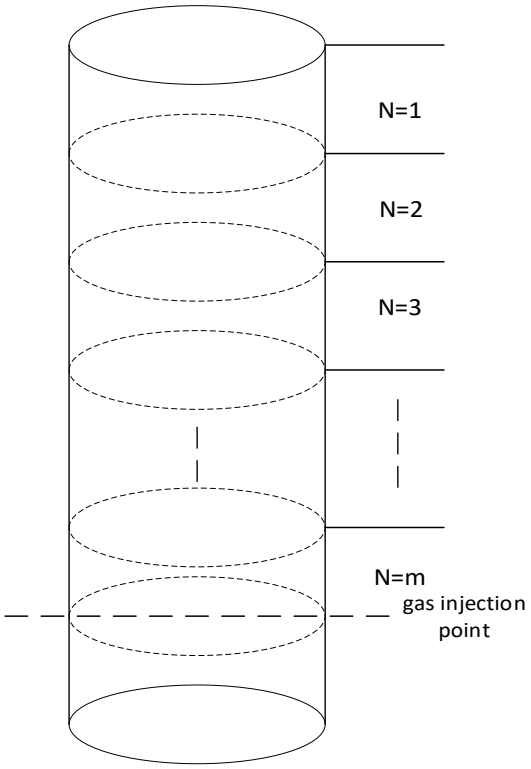

Figure 2. Schematic of Grid Division in Gas–Liquid Two-Phase Flow Section.

The process of calculating the injection point pressure and bottom-hole pressure is shown in Figure 3. First, the drill string is divided, followed by gas–liquid two-phase flow calculations. Iterative calculations are performed starting from the wellhead until the injection point is reached. After that, single-phase flow calculations are conducted from the injection point to the bottom-hole.

The calculation process for gas–liquid two-phase flow is shown in Figure 4. The top pressure and temperature of the divided infinitesimal units are used to calculate the gas holdup, gas phase density, mixed phase density, and other parameters using the formulas

from Section 2. This allows for the determination of the bottom temperature and pressure of each infinitesimal unit. These temperature and pressure values are then used as the initial conditions for the next unit's calculations, continuing until the injection point is reached and the calculation is complete.

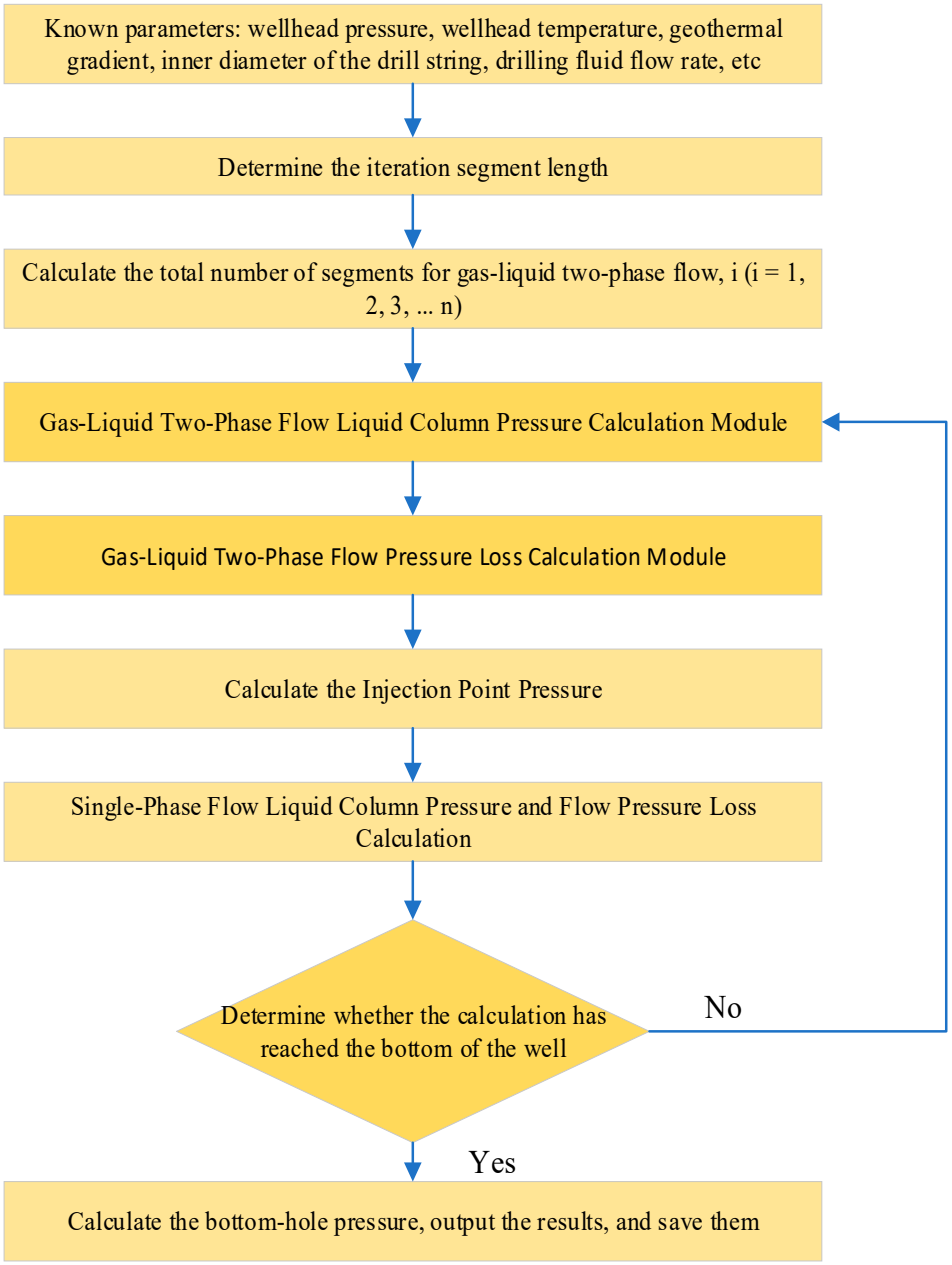

Figure 3. Flowchart of Gas-Lift Reverse Circulation Pressure Calculation Method.

The discretization step length ΔL is set to 10 m for all simulations. This value was chosen after a grid independence study: reducing ΔL to 5 m changed the bottom-hole pressure by less than 0.1%, while increasing ΔL to 20 m resulted in a 1.2% difference. The convergence criterion for the iterative pressure calculation in each grid cell is set to 1×10^{-4} MPa. The iteration loop terminates when the difference between two consecutive pressure estimates falls below this threshold. These parameters ensure numerical accuracy without excessive computational cost.

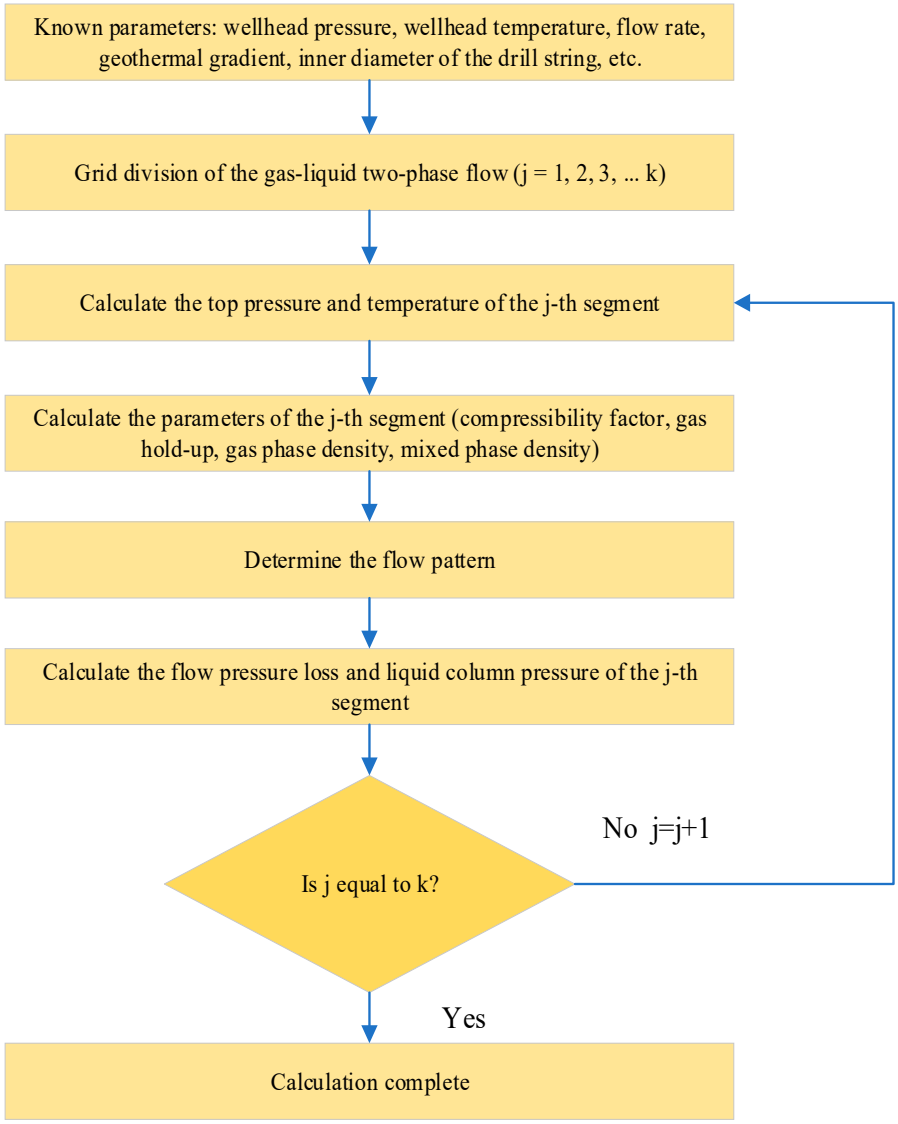

Figure 4. Liquid Column Pressure and Flow Pressure Loss Calculation Module.

4. Case Study Analysis

Analyze and explain the case study based on the constructed model and calculation method.

4.1. Basic Parameters

The basic data for the case study is referenced from the field data of a shale gas well in the southern Sichuan region. The data is as follows: the drilling fluid density is 1 g/cm^3, the drilling fluid viscosity is 1 mPa·s, the gas density is 1.21 kg/m^3, the geothermal gradient is 3 °C/100 m, the wellhead temperature is 20 °C, the wellhead pressure is 0.1 MPa, and the inner diameter of the drill string is 0.08 m.

The drilling fluid in the case study is assumed to be a Newtonian fluid with a viscosity of 1 mPa·s (water-like) for simplicity. This assumption is acceptable for low-solids, low-viscosity drilling fluids used in some lost circulation scenarios.

4.2. Calculation Result Analysis

4.2.1. Flow Pattern Analysis at Different Gas Injection Rates

First, a flow pattern analysis within the drill string is conducted. As shown in Figure 5, when the gas injection rate is between 150 and 240 L/s, the gas–liquid two-phase flow pattern within the drill string consists of a co-existence of bubbly flow and slug flow.

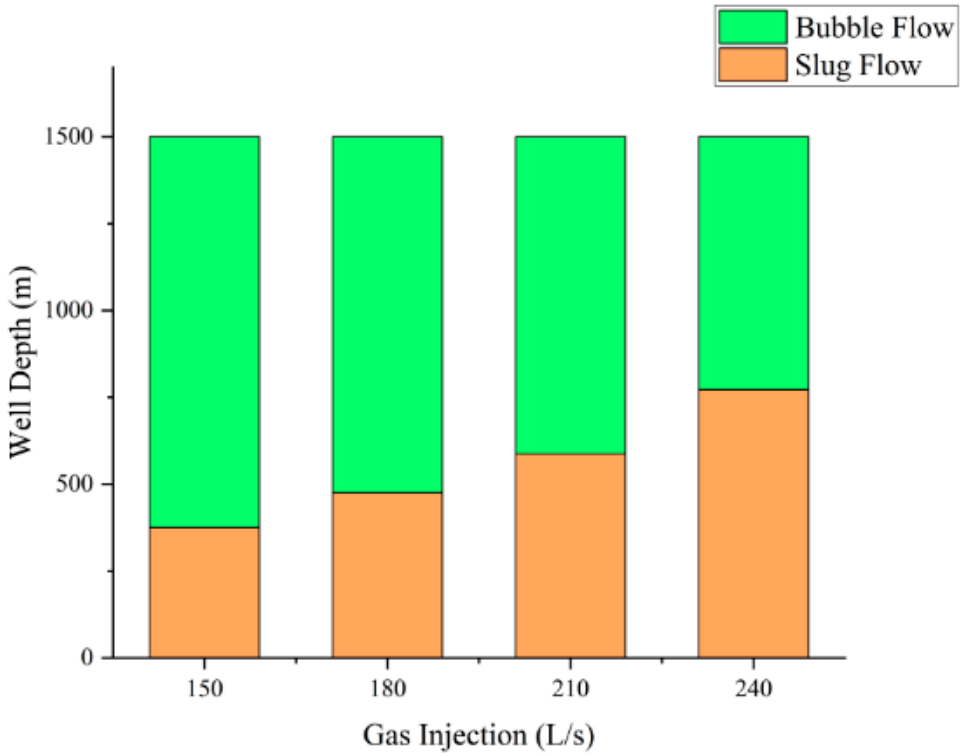

Figure 5. Flow Pattern Changes at Different Gas Injection Rates.

When the gas injection rate is 150 L/s, bubbly flow transitions to slug flow at a depth of 375 m; when the gas injection rate is 180 L/s, bubbly flow transitions to slug flow at a depth of 475 m; when the gas injection rate is 210 L/s, bubbly flow transitions to slug flow at a depth of 587.5 m; and when the gas injection rate is 240 L/s, bubbly flow transitions to slug flow at a depth of 772 m. As shown in Figure 5, for the same injection point, as the gas injection rate increases, the proportion of bubbly flow gradually decreases. This is because, with the increase in gas injection rate, the relative velocity of the gas increases, and the volume and number of bubbles in bubbly flow gradually increase. The flow conditions of the gas–liquid two-phase mixture inside the drill string start to intensify, and the gas–liquid phase interface is gradually disturbed. More irregular bubbles begin to appear in the drill string. Due to the increased disturbance and gradual accumulation, some bubbles come into contact and merge into larger gas masses with different characteristics. In other words, as the apparent velocity of the gas phase increases, the dispersed gas bubbles, which are more prone to disturbance, coalesce into larger bubbles, eventually evolving into slug flow.

From a mathematical and physical perspective, this downward shift in the transition point can be explained by the coupling between superficial gas velocity and hydrostatic pressure gradient. As the gas injection rate increases, the superficial gas velocity rises proportionally, leading to a higher void fraction. The increased gas holdup reduces the mixture density, thereby decreasing the local hydrostatic pressure gradient. Consequently, a longer vertical distance is required to accumulate the pressure differential necessary to reach the critical transition velocity for slug flow. Physically, the increased bubble population promotes coalescence, but the lower mixture density delays the formation of stable Taylor bubbles until a deeper location where higher ambient pressure compresses the gas and restores a sufficient density gradient. This interplay between flow regime transition criteria and wellbore pressure profile fully accounts for the observed trend in Figure 5.

4.2.2. The Impact of Different Gas Injection Points on Bottom-Hole Pressure

At a well depth of 2500 m and a gas injection rate of 150 L/s, the impact of different drilling fluid flow rates and gas injection point positions on bottom-hole pressure is analyzed. As shown in Figure 6a, it can be observed that when the drilling fluid flow rate increases, the bottom-hole pressure also increases. As the gas injection point is lowered, the bottom-hole pressure decreases accordingly, with a relatively gentle downward trend.

At a well depth of 2500 m and a drilling fluid flow rate of 20 L/s, the impact of different gas injection rates and gas injection point positions on bottom-hole pressure is analyzed. As shown in Figure 6b, when the gas injection point position and drilling fluid flow rate are the same, an increase in gas injection rate leads to a gradual decrease in bottom-hole pressure. Moreover, as the gas injection rate increases, the change in bottom-hole pressure becomes more pronounced. Taking gas injection rates of 160 L/s and 240 L/s as examples: when the gas injection rate is 160 L/s, as the injection point deepens, the bottom-hole pressure decreases from 25.35 MPa to 21.87 MPa, a reduction of 13%. When the gas injection rate is 240 L/s, as the injection point deepens, the bottom-hole pressure decreases from 24.28 MPa to 19.58 MPa, a reduction of 19%.

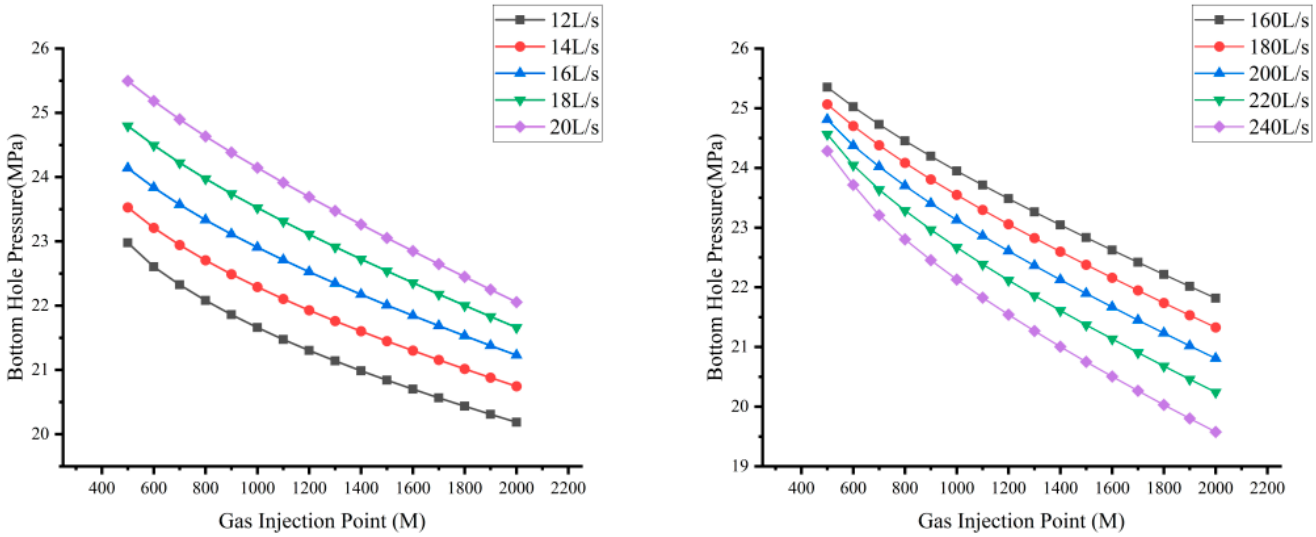

(**a**) (**b**)

Figure 6. Relationship between gas injection point position and bottom-hole pressure: (**a**) different flow rates; (**b**) different gas injection rates.

This is because, in gas-lift reverse circulation drilling, as the gas injection point deepens, the proportion of gas in the drill string increases. The deeper the well, the higher the liquid pressure. Therefore, the effect of gas injection becomes more significant. In the gas–liquid two-phase flow formed after gas injection, the gas gradually occupies an increasing volume, which further reduces the density and pressure of the liquid column.

To better understand the pressure reduction mechanism, the total bottom-hole pressure decrease can be decomposed into hydrostatic and frictional components. Taking the case with injection point at 1000 m and gas injection rate increasing from 150 L/s to 240 L/s, the total bottom-hole pressure decreases by 2.1 MPa. Of this reduction, approximately 1.7 MPa (81%) is attributed to the decrease in hydrostatic column density (due to increased gas holdup), while the remaining 0.4 MPa (19%) is due to changes in frictional pressure loss (which actually increases slightly with gas rate but is offset by density reduction). This decomposition confirms that the primary mechanism of pressure reduction in gas-lift

reverse circulation is hydrostatic density reduction, not friction loss modification. For deeper injection points, the hydrostatic contribution becomes even more dominant because the longer two-phase column amplifies the density effect.

4.2.3. The Impact of Different Gas Injection Rates on Bottom-Hole Pressure

At a well depth of 2500 m and a drilling fluid flow rate of 14 L/s, the variation in bottom-hole pressure under different gas injection rates is shown in Figure 7a. As can be seen from Figure 7a, as the gas injection rate increases, the bottom-hole pressure continuously decreases. Moreover, as the injection point deepens, the impact of the gas injection rate on the bottom-hole pressure becomes more significant. Taking injection points at 800 m and 1600 m as examples, when the injection point is at a depth of 800 m, the bottom-hole pressure decreases from 22.9 MPa to 20.98 MPa, a reduction of 8%. When the injection point is at a depth of 1600 m, the bottom-hole pressure decreases from 21.56 MPa to 18.73 MPa, a reduction of 13%.

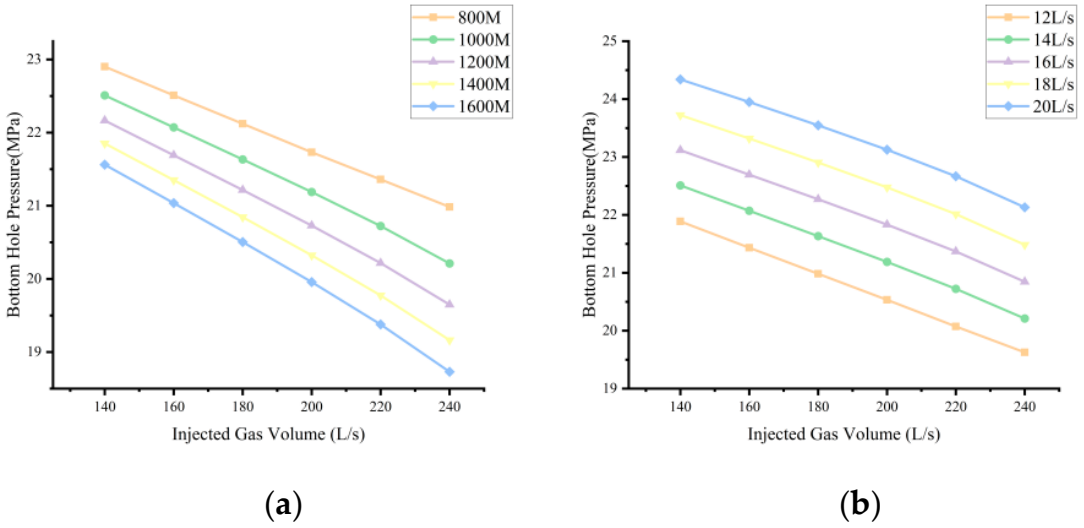

(**a**) (**b**)

Figure 7. Relationship between different gas injection rates, injection points, and bottom-hole pressure: (**a**) different gas injection points; (**b**) different flow rates.

At a well depth of 2500 m and a gas injection point position of 1000 m, the variation in bottom-hole pressure under different gas injection rates is shown in Figure 7b. As can be seen from Figure 7b, when the gas injection point position is the same, the bottom-hole pressure increases as the drilling fluid flow rate increases. However, by increasing the gas injection rate, the bottom-hole pressure can be reduced.

4.3. Application Analysis

The calculation results of the bottom-hole pressure prediction method for gas-lift reverse circulation developed in this study are compared with the results from the gas-lift reverse circulation drilling design and monitoring software used for a shale gas well in the southern Sichuan region. The comparison results are shown in Figure 8.

Under the same operating conditions, the bottom-hole pressure comparison curve for different gas injection point positions is shown in Figure 8a. It can be seen that the maximum error of the calculation results from the method established in this study is only 3%, corresponding to an absolute difference of less than 0.65 MPa (e.g., at injection point depth 1500 m, the software gives 20.8 MPa while the model gives 20.2 MPa, a difference of 0.6 MPa).

Under the same operating conditions, the bottom-hole pressure comparison curve for different gas injection rates is shown in Figure 8b. It can be seen that the maximum

error of the calculation results from the method established in this study is only 2.7%, corresponding to an absolute difference of less than 0.55 MPa.

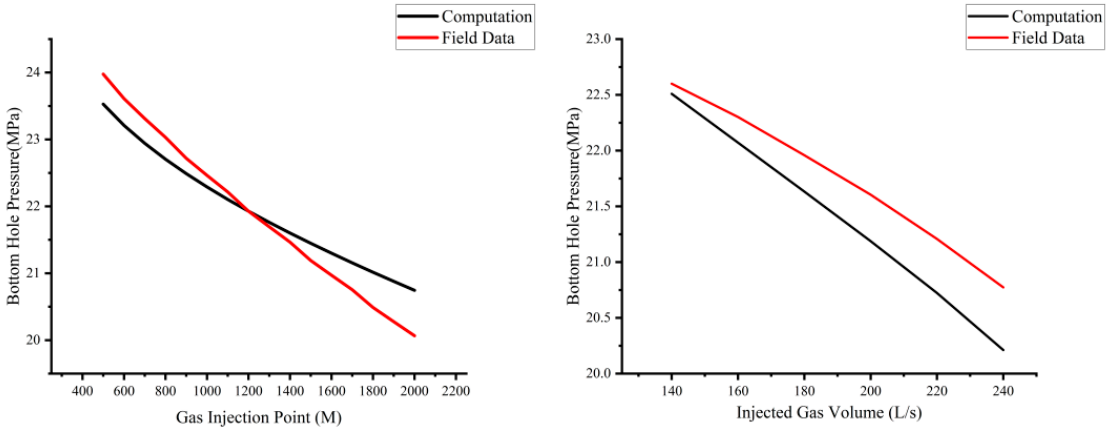

(**a**) (**b**)

Figure 8. Bottom-hole pressure comparison curve: (**a**) different gas injection points; (**b**) different gas injection rates.

By comparing the data, it is found that the relative error between the two is within 5%. Therefore, the gas-lift reverse circulation bottom-hole pressure calculation model developed in this study can predict the bottom-hole pressure with a high degree of accuracy.

5. Conclusions

This study proposes a new method for predicting bottom-hole pressure in gas-lift reverse circulation drilling. Based on the gas–liquid two-phase flow theory, a pressure calculation method suitable for gas-lift reverse circulation conditions is established. The finite difference principle is applied, and through reasonable grid division inside the drill string, iterative calculations are performed to analyze the bottom-hole pressure. The results show that

(1) In gas-lift reverse circulation drilling, the flow pattern of gas–liquid two-phase flow inside the drill string is primarily slug flow and bubbly flow. As the gas injection rate increases, the proportion of slug flow increases accordingly.

(2) When the well depth and drilling fluid flow rate are the same, as the gas injection point deepens, the bottom-hole pressure decreases. Furthermore, as the gas injection rate increases, the change in bottom-hole pressure becomes more pronounced.

(3) By analyzing the impact of different gas injection rates on bottom-hole pressure, it can be observed that as the gas injection rate increases, the bottom-hole pressure continuously decreases. Moreover, the deeper the injection point, the greater the reduction in pressure.

(4) The calculation method proposed in this study predicts bottom-hole pressure under gas-lift reverse circulation conditions with an error of less than 5% compared with field monitoring software. Beyond accurate prediction, the model provides actionable engineering guidance: (1) Optimal injection depth: To achieve a target bottom-hole pressure reduction of 3 MPa, the injection point should be placed deeper than 1000 m while maintaining a gas injection rate of at least 180 L/s. (2) Gas injection efficiency: Increasing the gas injection rate beyond 240 L/s yields diminishing returns in pressure reduction while elevating the risk of wellhead erosion and annular flow instability. (3) Real-time control strategy: When formation fluid influx increases, operators should prioritize raising the gas injection rate over the liquid pump rate,

as the model demonstrates a 13% greater pressure reduction per unit increase in gas flow at deeper injection points.

The calculation method studied in this paper can predict the bottom-hole pressure under gas-lift reverse circulation conditions, solving the problem of insufficient accuracy when using empirical formulas to predict bottom-hole pressure in conventional gas-lift reverse circulation drilling. This is of significant importance for the development of gas-lift reverse circulation technology in the oil and gas well field.

Author Contributions: Conceptualization, P.L. and C.G.; methodology, P.L.; software, R.Z.; validation, P.L., C.G. and R.T.; formal analysis, P.L.; investigation, C.G.; resources, S.F.; data curation, R.Z.; writing—original draft preparation, P.L.; writing—review and editing, C.G.; visualization, R.Z.; supervision, S.F.; project administration, R.T.; funding acquisition, P.L. All authors have read and agreed to the published version of the manuscript.

Funding: This research was funded by Sichuan Provincial Department of Science and Technology grant number 2024NSFSC202.

Institutional Review Board Statement: Not applicable.

Informed Consent Statement: Not applicable.

Data Availability Statement: The original contributions presented in this study are included in the article. Further inquiries can be directed to the corresponding author.

Conflicts of Interest: Author Ruifeng Tan was employed by the company Sinopec Huadong Oilfield Service Corporation. Author Shanquan Fan was employed by the company China National Petroleum Corporation Jidong Oilfield Company. The remaining authors declare that the research was conducted in the absence of any commercial or financial relationships that could be construed as a potential conflict of interest.

Nomenclature

P_{jd}	Bottom-hole pressure, MPa
P_0	Wellhead pressure, MPa
P_{yz}	Hydrostatic pressure of the fluid column inside the drill string, MPa
P_{yh}	Flow pressure loss inside the drill string, MPa
P_{qy}	Hydrostatic pressure of the liquid column in a gas–liquid two-phase flow, MPa
P_d	Hydrostatic pressure of the fluid column in the single-phase drilling fluid segment, MPa
ρ_m	Gas–liquid mixture density, kg/m^3
Δh	Height of the gas–liquid two-phase flow segment, m
E_g	Gas holdup, %
ρ_g	Gas density, kg/m^3
ρ_l	Drilling fluid density, kg/m^3
v_{sg}	Apparent velocity of the gas phase, m/s
v_g	Gas phase velocity, m/s
v_{sl}	Apparent velocity of the liquid phase, m/s
v_l	Liquid phase velocity, m/s
Q_g	Gas flow rate, m^3/s
Q_l	Liquid flow rate, m^3/s
A	Cross-sectional area of the inner diameter of the drill pipe, m^2
v_m	Mixed flow velocity of the gas–liquid two-phase flow, m/s
M_g	Air molar mass, kg/mol
R	Gas constant, 8.314 J/(mol·K)
Z	Gas compressibility factor.
$\frac{dp}{dz}$	Friction gradient term.
f_m	Fanning friction factor.

D Inner diameter of the drill pipe, m
h_2 Height from the gas–water mixer to the wellbore bottom, m
f_l Fanning friction factor for the single-phase drilling fluid segment.

References

1. Feng, Y.; Yang, H.; Li, X.; Zhang, S.; Hu, H.; Wang, J. Interpretable Lost Circulation Analysis: Labeled, Identified, and Analyzed Lost Circulation in Drilling Operations. *SPE J.* **2024**, *29*, 1692–1709. [CrossRef]
2. Li, C.; Wu, Z.; Huang, Z.; Guan, Z.; Cao, J.; Dong, G.; Xu, H. Failure risk assessment of deepwater HTHP well completion test string based on uncertainty analysis. *Pet. Sci. Technol.* **2022**, *42*, 597–612. [CrossRef]
3. Ai, X.; Chen, M. Wellbore Stabilization Technology of "Fluid-Solid-Chemical Coupling" in Continental Shale Oil—A Case Study of Shale Oil in Block GL. *Energies* **2022**, *15*, 6962. [CrossRef]
4. Ren, J.; Xu, P.; Xu, M.; Zhang, Y.; Wang, X. Research on the Development and Plugging Capacity of a Honeycomb Porous Lost-Circulation Material. *ACS Omega* **2022**, *7*, 21624–21629. [CrossRef]
5. Luo, Y.; Guo, B.; Zhang, L.; Xiao, D. Finite Element Analysis of Flow Field in Drill Bit Design for Gas-Lift Drilling. *J. Energy Resour. Technol.* **2021**, *143*, 113002. [CrossRef]
6. Ding, Y.; Liu, X.; Liang, L.; Xiong, J.; Li, W.; Wei, X.; Duan, X.; Hou, L. Wellbore stability model in shale formation under the synergistic effect of stress unloading-hydration. *Pet. Explor. Dev.* **2023**, *50*, 1478–1486. [CrossRef]
7. Kamiński, P. A New Method of Regulation of Loads Acting on the Shaft Lining in Sections Located in the Salt Rock Mass. *Energies* **2020**, *14*, 42. [CrossRef]
8. Wang, T.; Wei, Q.; Xiong, W.; Wang, Q.; Fang, J.; Wang, X.; Liu, G.; Jin, C.; Wang, J. Current Status and Prospects of Artificial Intelligence Technology Application in Oil and Gas Field Development. *ACS Omega* **2024**, *9*, 3173–3183. [CrossRef]
9. Guo, L.; Cheng, H.; Yao, Z.; Rong, C.; Lin, J.; Wang, X. Mathematical model of velocity and distribution law in gas lift reverse circulation well washing flow field for drilling shaft sinking. *Sci. Rep.* **2024**, *14*, 27327. [CrossRef]
10. Wang, J.; Deng, S.; Li, J.; Yang, H.; Liu, G. Development of a multiphase variable mass flow model and its application in well control for variable gradient managed pressure drilling. *Energy Rep.* **2023**, *9*, 3358–3368. [CrossRef]
11. Yang, H.; Li, J.; Liu, G.; Xing, X.; Jiang, H.; Wang, C. The effect of interfacial mass transfer of slip-rising gas bubbles on two-phase flow in the vertical wellbore/pipeline. *Int. J. Heat Mass Transf.* **2020**, *150*, 119326. [CrossRef]
12. Zheng, J.; Dou, Y.; Li, Z.; Yan, X.; Zhang, Y.; Bi, C. Investigation and application of wellbore temperature and pressure field coupling with gas–liquid two-phase flowing. *J. Pet. Explor. Prod. Technol.* **2021**, *12*, 753–762. [CrossRef]
13. Salubi, V.; Mahon, R.; Oluyemi, G.; Oyeneyin, B. Effect of two-phase gas-liquid flow patterns on cuttings transport efficiency. *J. Pet. Sci. Eng.* **2022**, *208*, 109281. [CrossRef]
14. Zhang, W.; Xue, X.; Zhang, C.; Qu, Y.; Ke, K.; Pan, S.; Li, Z.; Zhang, J. A drilling wellbore pressure calculation model considering the effect of gas dissolution and suspension. *Front. Earth Sci.* **2022**, *10*, 993876. [CrossRef]
15. Tian, J.; Song, X.; Li, D.; Cao, G.; Wang, X.; Wang, Y.; Meng, S. Pressure changes in two-phase flow of gas and liquid in a wellbore. *J. Phys. Conf. Ser.* **2024**, *2756*, 012034. [CrossRef]
16. Zheng, J.; Li, Z.; Dou, Y.; Zhang, Y.; Bi, C.; Yang, X.; Li, J. Study on Downhole Throttling Characteristics of High Water Content Gas. *Geofluids* **2022**, *2022*, 5257771. [CrossRef]
17. Wei, N.; Pei, J.; Xue, J.; Jiang, L.; Li, H.; Sun, W.; Zhang, Y. Modeling of multiphase flow during underbalanced drilling considering velocity, temperature and pressure. *Energy Rep.* **2022**, *8*, 2574–2587. [CrossRef]
18. Dindoruk, B.; Zhang, F. Advances in Drilling and Completion Fluid Technologies for Protecting Oil and Gas Reservoirs: Research Progress and Development Trends. *J. Energy Resour. Technol.* **2024**, *146*, 050801. [CrossRef]
19. Yang, J.; Sun, J.; Bai, Y.; Lv, K.; Zhang, G.; Li, Y. Status and Prospect of Drilling Fluid Loss and Lost Circulation Control Technology in Fractured Formation. *Gels* **2022**, *8*, 260. [CrossRef]
20. Hu, Y.; Yang, Y. A Comparative Study on Drag Reduction Methods for Continental Shale Drilling in the Fuxing Block, Southeastern Sichuan Basin. *Reserv. Sci.* **2026**, *2*, 81–96. [CrossRef]
21. Tian, L.; Zhang, Q.; Li, X.; Li, C. Fracturing Effectiveness Evaluation Based on Flowback Data Using Pressure Transient Testing. *Reserv. Sci.* **2026**, *2*, 97–110. [CrossRef]
22. Nwaka, N.; Wei, C.; Ambrus, A.; Chen, Y. Gas in riser: On modeling gas influxes in non-aqueous drilling fluids with time-dependent desorption considerations. *J. Pet. Sci. Eng.* **2020**, *195*, 107785. [CrossRef]